JOURNAL OF SPACECRAFT AND ROCKETS
Vol. 47, No. 6, November–December 2010

Imaging and Slitless Spectroscopy of the Stardust Capsule Reentry Radiation

Franziska Harms*
Kayser–Threde, GmbH, 81379 Munich, Germany
Juergen Wolf†
University of Stuttgart, 70569 Stuttgart, Germany
George Raiche‡
NASA Ames Research Center, Moffett Field, California 94035
and
Peter Jenniskens§
SETI Institute, Mountain View, California 94043

DOI: 10.2514/1.38054

Observations were made during the reentry of the Stardust sample return capsule on 15 January 2006 in order to calibrate the level of radiation from the capsule surface, from the bow shock, and from its wake. A sensitive cooled charge-coupled device camera was used, equipped with a grating to simultaneously record the first-order spectrum of the capsule and that of the background stars. The radiation of the capsule was dominated by the graybody radiation from the hot surface. This graybody radiation was calibrated against the known radiation of background stars. The purpose of this calibration was to provide a cross check for other instruments participating in the airborne Stardust Entry Observing Campaign. In addition, eight short-exposed images were obtained that show the development of billowing and the distortion induced by winds.

I. Introduction

THE reentry of the Stardust sample return capsule (SRC) was the fastest reentry of a vehicle into the Earth's atmosphere to date and was observed by a range of spectroscopic instruments onboard a NASA DC-8 aircraft: the Stardust Entry Observing Campaign [1]. Stardust was NASA's mission to bring back a sample of cometary dust collected at comet 81P/WILD 2. The return trajectory was similar to that of a natural asteroid, and the capsule entered Earth's atmosphere at a speed of 12.8 km/s (at 135 km altitude). The research aircraft was positioned at the end of the shallow entry trajectory, close to the landing site at the Utah test and training range. The aircraft provided a clear view of the reentry radiation and monitored most of the reentry path.

Radiation signatures from the capsule's hot surface, shock emissions, and the material ablating from the heat shield were detected by a range of different instruments that covered various parts of the electromagnetic spectrum between 320 and 1450 nm.

Our instrument recorded the optical spectrum between 400 and 900 nm at low resolution but with high dynamic range, and in a manner so that the spectra of the background stars were simultaneously measured. This enabled us to calibrate the intensity of the radiation using internal calibration from the known flux values of the background stars. This work was executed as part of our effort to gain experience with sensor calibration processes [2]. Here we report on the instrument definition and the process of calibration against the background stars.

Another unique aspect of our observations was the ability to image the chemiluminescent wake of the capsule.

II. Instrument

We used a SBIG ST-10XME camera [3] with a cooled Kodak KAF-3200ME charge-coupled device (CCD) of 2184 by 1472 pixels with the size of 6.8 μm (Fig. 1). The camera was equipped with a Nikon f/2.8, 180 mm lens that provided a field of view of 4.74× 3.18°. Images were obtained 2 × 2 binned to reduce the readout time. The image scale on the sky was 15.62 arcsec for one binned pixel. The exposure time was set to the minimum time of 0.1 s. The readout time of one image was about 5.5 s, so that we could take one image every 5.5 s.

A grating was mounted just in front of the imaging plane and had 500 lines per millimeter. This geometry allowed us to record spectra only from light sources inside the field of view of the grating (and projected onto the CCD after diffraction), so that there was no background contamination from sources elsewhere.

The source was not spatially resolved and appeared as a point source, just as the background stars. The light was not collimated; thus, the focus changed over the range of wavelengths.

A less sensitive CCD camera with a higher readout time and larger field of view (∼9 × 14°) was mounted to the ST-10 and connected to a video headset for tracking purposes. The camera was installed on the aircraft fixed mounting platform, allowing manual tracking in one axis. The tracking angle on the sky was selected in such a way that the SRC could be tracked for most of its reentry trajectory.

III. Instrument Definition and Data Extraction

The position of the spectrum on the CCD depends on the position of the capsule in the field of view. To derive the wavelength of a given pixel, it is necessary to calibrate the wavelength scale and use the image of the capsule in zero order (or a known emission line in the first order) as reference [4]. Once the wavelength scale is calibrated, we can compare the observed intensity along the spectrum with that of the spectra of the background stars.

Presented as Paper 2008-1214 at the 46th AIAA Aerospace Sciences Meeting and Exhibit, Reno, NV, 7–10 January 2008; received 15 April 2008; revision received 16 August 2010; accepted for publication 19 August 2010.

*Systems Engineer, Wolfratshauserstrasse 48.
†Senior Research Scientist, Deutsches SOFIA Institut, Pfaffenwaldring 31.
‡Branch Chief, Thermophysics Facility Branch, Mail Stop N229-4.
§Research Scientist, Principal Investigator, Carl Sagan Center, 515 North Wisman Road. Member AIAA.

Fig. 1 The cooled CCD camera and tracking camera, as installed on the aircraft.

A. Extraction of Spectrum

A dark current background was subtracted from the CCD images using 32 median-averaged dark field images that were acquired before and after the SRC observation. Column defects and hot pixels were removed by replacing the corresponding pixels by the averaged intensity of neighboring pixels. The resulting images are shown in Fig. 2, along with the Universal Time Coordinated (UTC) start times of the exposure. The images are aligned to a sky map by means of identified stars in the images. The first acquired spectrum at 09:57:08.5 UTC is not shown due to overlap. The images at 09:57:14.0 and 09:57:19.5 UTC show the first-order spectra of the SRC, and the images at 09:57:25.0 and 09:57:30.0 UTC show the zero-order image and the first-order spectra.

The star spectra used in our calibration are those of the Pleiades cluster, detected in the exposure starting at 09:57:19 UTC, which included the stars 25-, 27-, 23-, 17-, 19-, and 20- Tau. The star spectra were detected in the opposite first order from that of the capsule.

A bright moon created a relatively strong sky background that was subtracted from the images. Nearby rows were averaged on both sides of the spectra, fitted by a third-order polynomial and subtracted from the main intensity curve. The two spectra recorded at 09:57:25 and 09:57:30 UTC are additionally affected by scattered light of the zero-order image. An exponential fit is determined by the intensity curve of the zero-order image, extended over the length of the first-order spectrum and subtracted from the main intensity curve, eliminating the effect of the scattered light on the spectral data. Finally, the result was divided by a flat-field spectrum to remove pixel-by-pixel sensitivity variations. The flat-field spectrum was produced using a dark-field-corrected and background-subtracted image of the dark sky recorded earlier that night.

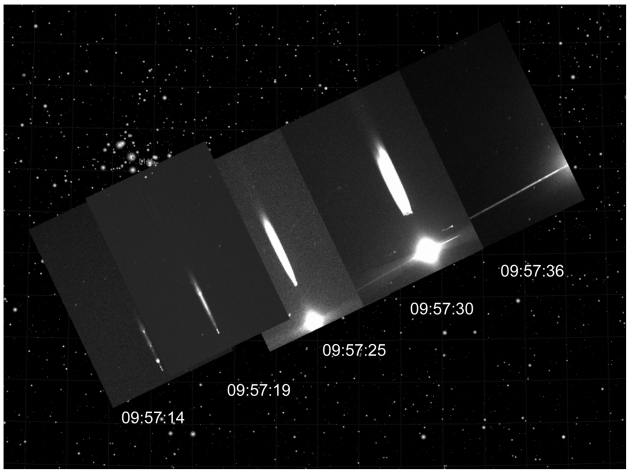

Fig. 2 Low-resolution spectra of the SRC and UTC start times of the exposure. The Pleiades star cluster is visible on the upper edge of the image at 09:57:19 UTC.

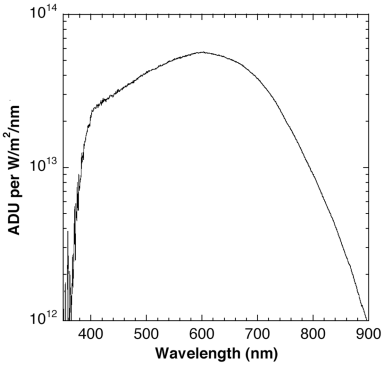

Fig. 4 Spectral response curve of the instrument (for SRC entry observations). The asterisk denotes the 2 × 2 binning aperture 2.8, 0.1 s exposure.

The spectra were extracted by summing up the intensity perpendicular to the dispersion direction. The spectrum was dispersed by 25–90 pixel rows, depending on its intensity, more so at the edges of the spectrum. The result is the pixel intensity in counting units versus pixel position.

B. Wavelength Calibration

The wavelength calibration was performed with an Ocean Optics HgAr wavelength calibration lamp to measure the dispersion of the grating. We obtained 1 × 1 binned calibration images. The lamp was placed outside the aircraft at a distance of 2.46 m. We used vacuum wavelengths published in the Kurucz tables for the Hg and Ar lines. We measured a dispersion of 1.7 nm per binned pixel. From the width of the emission lines in the spectra, we measured a wavelength resolution of about 10 nm at 480 nm wavelength (Zn lines).

C. Instrumental Response Curve

In addition, we observed a LS-1-CAL tungsten–halogen calibration lamp (LSC1429) [5], with no fiber (3 mm ø), during tarmac tests from a distance of 2.46 m, through the aircraft window to measure the instrument response curve. The distance to the lamp was measured from the size of the image of the lamp housing on the CCD. The lamp used was newly acquired from the factory, which provided a calibration curve in units of flux falling into a fiber placed just above the Lambert diffuser Teflon surface, seen through the 3 mm aperture. The observed flux was corrected for solid angle, π (1.5/2460) [2]. We also took into account the factor 6.496, which is the solid angle of the fiber used to calibrate this lamp.

The continuum source was placed immediately below the wavelength calibration lamp, so that both sources were observed at the same time (Fig. 3). Zero-order images of both lamps provided the zero reference of the wavelength scale. Background subtraction and scattered light of the lamp were eliminated from the intensity curve, as described in Sec. III.A.

Fig. 3 Example of calibration image.

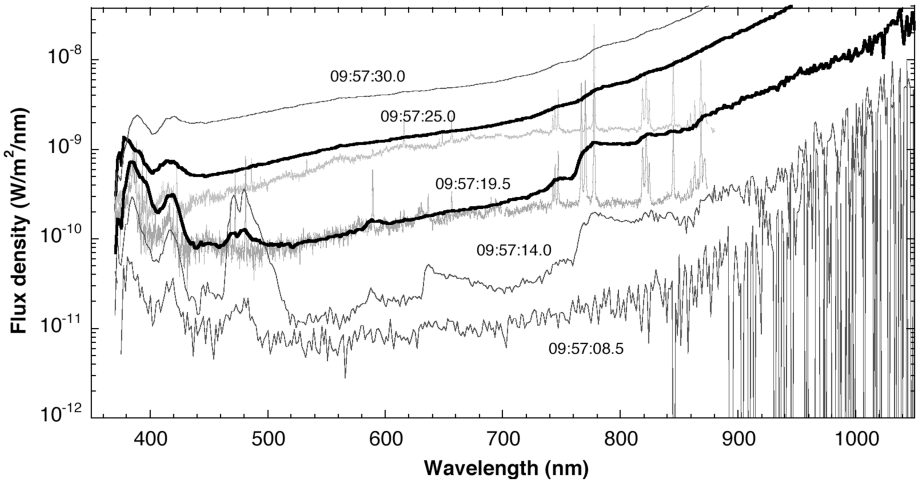

Fig. 5 Extracted spectra in logarithmic scale. Wavelength and intensity calibrated. Our results are compared with two spectra obtained by the echelle spectrograph.

We divided the wavelength-calibrated intensity curve by the lamp flux to obtain the instrumental spectral response curve. This includes the window transmission but not atmospheric extinction. The angle through the window was similar to that of the later SRC reentry measurements. The calibration curve extracted from this, given the known emission from the tungsten source, provided the instrument response curve, shown in Fig. 4.

The measurements were made at an exposure time of 0.1 s, an aperture stop of $f/22$, and 1×1 binning, and they were then scaled to apply to the response for the SRC entry observations: 0.1 s exposure time, aperture stop of $f/2.8$, and 2×2 binning.

IV. Calibration of Extracted Spectra

A. Wavelength Calibration

We performed an internal wavelength calibration of the five extracted spectra by identifying emission lines of CN, Ca, Zn, Na, O, K, and N. The wavelength values of the identified emission lines were assigned to the according pixel locations on each image. A second-order polynomial least-squares fit yields the relation between pixel number and wavelength. We calibrated the extracted spectra with this curve. The result was the relative intensity in counting units versus the wavelength.

The wavelength calibration performed with the identified emission lines differed slightly from the wavelength calibration performed with the calibration lamp toward larger wavelengths. At a wavelength of 800 nm, the deviation between the two calibration curves was about 8%. The effect is explained by the difference in the focal length of the lens, because we focused on the nearby lamp during calibration and had to change the focus to infinity for the SRC reentry observation.

B. Intensity Calibration

For absolute flux calibration, we divided the wavelength calibrated flux profile [in counting units, analog-to-digital units (ADUs)] by the measured spectral response curve (Fig. 4). The response curve was fitted by a series of second- and third-order polynomials to match the curve to the measured wavelengths for each pixel.

C. Results

The five resulting Stardust SRC entry flux spectra in units of $W/m^2/nm$ versus wavelength are shown in Fig. 5. These flux data are measured at the location of the airplane and have been corrected for atmospheric extinction, calculated using MODTRAN (moderate resolution atmospheric transmission computer program) for the known altitude of the aircraft and elevation of the capsule at each moment. The SRC position as seen from the DC-8 aircraft during each exposure is listed in Table 1.

The result is compared with data obtained by an echelle spectrograph, which was a separate instrument deployed in the Stardust Entry Observing Campaign [5]. Two averages of echelle spectra were measured between 09:57:19.0 and 09:57:20.0 UTC and measured between 09:57:24.5 and 09:57:25.5 UTC (gray lines in Fig. 5 that terminate at 880 nm). The first average should correspond to our third spectrum in the middle of Fig. 5. The agreement is very good below 580 nm, but our data show a continuing increase in continuum emission toward longer wavelengths that is not measured by echelle. That rise is also not seen in near-infrared (IR) observations of the capsule with a near-IR spectrometer [6]. Some of the increase toward shorter wavelength may be due to the strong atomic lines of K, O, and N, but the rise is also evident in the later spectra that have weak shock emissions. The cause of this rise in our data is not understood, but we suspect it may have to do with the spectra being out of focus differently between tarmac tests and Stardust SRC entry observations.

The second average should correspond to our fourth spectrum, counted from below. The echelle data and our data have an offset that is not understood. The general shape of the curves are in good agreement below 700 nm. Again, an increase in flux is observed above 700 nm that is not present in the echelle data.

V. Absolute Calibration with Star Spectra

As a verification of the absolute calibration, we derived the instrument spectral response from the recorded spectra of stars in the Pleiades cluster (Fig. 6).

The images obtained at 09:57:14 and 09:57:19 UTC (second and third spectrum from below, in Fig. 5) recorded the SRC spectra along

Table 1 SRC position as seen from the DC-8 aircraft

UTC	Azimuth, deg	Elevation, deg	Range, km	Azimuth rate, deg/s	Elevation rate, deg/s	Range rate, km/s
09:57:08.5	253.76	6.61	514.04	0.16	0.11	−12.26
09:57:14.0	254.60	7.27	446.76	0.17	0.14	−12.19
09:57:19.5	255.79	8.13	380.07	0.25	0.18	−12.02
09:57:25.0	257.48	9.28	314.69	0.28	0.24	−11.65
09:57:30.0	259.83	10.71	257.74	0.59	0.33	−10.96

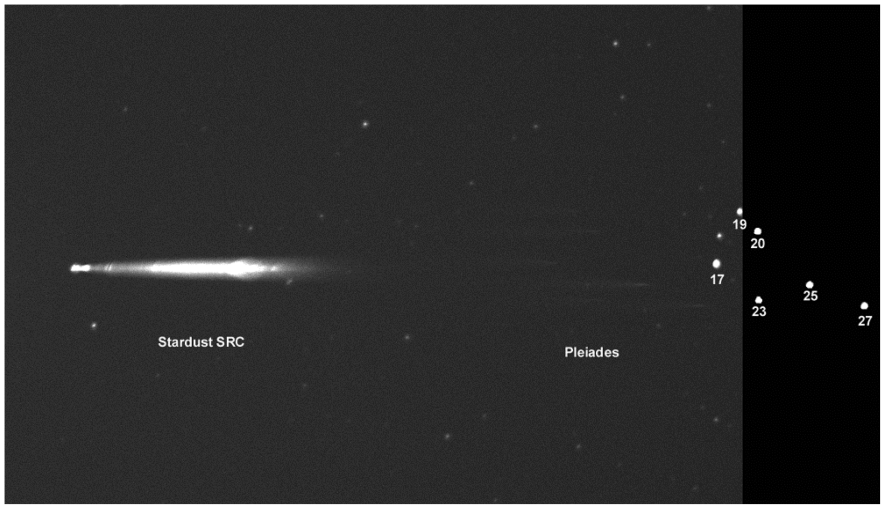

Fig. 6 First-order spectrum of the Stardust SRC at 09:57:19 UTC (left) and the Pleiades cluster stars (right). Only 17- and 19- Tau zero-order images are in the exposure. The zero-order images of the other Pleiades stars are added on the black background, providing a reference for the first-order star spectra. The first-order star spectra were detected in the opposite first order from that of the capsule.

with spectra of the Pleiades stars. The stars were at a 21° elevation. Similar to the SRC data reduction, the spectrum of the brightest star, 25- Tau, was extracted from each image by summing up the intensity values of a 31-pixel-wide area along the spectra. The sky background and scattered light of the SRC were subtracted from the intensity curve. The wavelength scale was measured from the Stardust SRC spectral emission lines and matched to the zero-order star images.

To yield the instrument's spectral response, the observed spectral distribution is divided by a reference spectrum for B7IIIe stars [7] [scaled to an absolute measure of flux outside Earth's atmosphere, using broadband photometric values listed in the SIMBAD (set of identifications, measurements, and bibliography for astronomical data) astronomical database]. The star spectrum was corrected for extinction with an extinction curve for the aircraft altitude, and the star elevation was calculated using MODTRAN.

Because the stars are dispersed in an opposite direction from the calibration and reentry images, an intensity correction was applied. We evaluated images with the star, Capella, in the image center, compared its spectra on both sides, and found a correction factor of 1.30 ± 0.05. The resulting spectral response curve is shown in Fig. 7.

The response derived from the star spectra is in good agreement with the response curve obtained with the calibration lamp below 530 nm, where the star spectra are brightest. Our observations confirm that the short-wavelength part of the echelle spectrum, dominated by CN and some N_2^+ molecular band emission, is not significantly contaminated by a background of scattered light.

Above 580 nm, the star spectra suggest a response curve slightly higher than the response measured with the calibration lamps. This would bring our observations in better agreement with the echelle spectra. Unfortunately, the star spectra are weak in this wavelength regime, and the signal is noisy (the error of the response curve gets as large as three orders of magnitude), so we refrained from recalculating the result with this new curve.

We tested if this discrepancy could be due to overlap in the second-order response above $2 \times 380 = 760$ nm. We placed a high-pass filter in the optical path and found only a negligible (less than 10%) contribution from the second-order emission. The grating put most light in the first order.

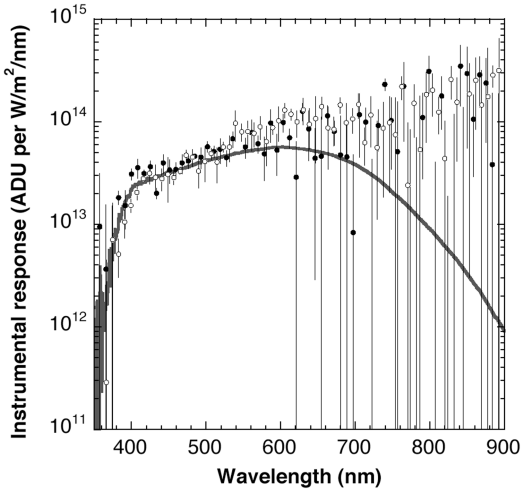

Fig. 7 Comparing the instrument spectral response derived from the observed star spectrum of 25- Tau at 09:57:14 (●) and 09:57:19 (○) UTC, with error bars and from the calibration lamp (solid line).

VI. Wake Imaging

We obtained a series of eight images of the wake of the SRC at an altitude of about 65 km over the time period from 09:57:30 to 09:58:15 UTC. One example is shown in Fig. 8. The wake width was about 10 pixels, or 156 arcsec, at a distance of 257 km that corresponded to a width of 194 m 12 s after the passing of the capsule.

The width did not change significantly over the period of observation, presumably because the hot-air column was in pressure equilibrium with its surroundings. We did observe an increase in the level of billowing and distortions due to upper atmosphere winds.

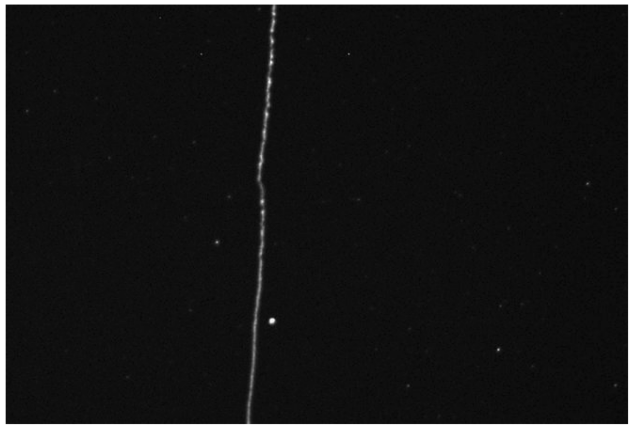

Fig. 8 Wake of the SRC.

VII. Conclusions

The reentry of the Stardust SRC was observed by a range of spectroscopic instruments onboard a NASA DC-8 aircraft. This paper presents the observations that were made with a sensitive cooled CCD camera equipped with a grating in order to record the optical spectrum of the reentry radiation between 400 and 900 nm. Five images were acquired that show the first-order spectra of the SRC. The extracted spectra were wavelength- and intensity-calibrated and represent the radiation flux measured at the location of the airplane. The radiation of the capsule was dominated by the graybody radiation from the hot surface. The results are compared with data obtained by an echelle spectrograph, a separate instrument deployed in the Stardust Entry Observing Campaign. The agreement of the measured radiation spectra is very good below 580 nm, and the general shape of the curves is in good agreement below 700 nm. However, our data show a continuing increase in continuum emission toward longer wavelengths that is not measured by the echelle spectrograph. Star spectra of a background star in the Pleiades cluster were simultaneously imaged. The known star spectra were used to derive the instrument spectral response as a verification of the absolute calibration. The response derived from the star spectra is in good agreement with the response curve obtained with the calibration lamp below 530 nm, where the star spectra are brightest. Toward longer wavelengths, the star spectra imply a slightly higher response curve, which brings our observations in better agreement with the echelle spectra. After the passing of the SRC, eight short-exposed images of the wake of the SRC were obtained at an altitude of about 65 km. The wake width was measured to be about 194 m and did not change significantly over the observation period of 45 s. The exposures showed the development of billowing and the distortion induced by winds.

Acknowledgments

F. Harms was supported by the Institute of Space Systems (University of Stuttgart), the Stratospheric Observatory for Infrared Astronomy project, the Gottlieb–Daimler and Carl–Benz Foundation, and Zonta International. The mission was funded and managed by the NASA Engineering and Safety Center. F. Harms would like to thank the colleagues at the Institute of Space Systems for fruitful discussions and great collaboration. The authors thank Jeff Ignaitis of M and O Precision Machine and Manufacturing for manufacturing the support structure. Haiping Su of the Airborne Science and Technology Lab at NASA Ames Research Center provided the MODTRAN extinction calculations. We also thank Jim Albers of Lockheed Martin for helping identify the star background in our images. NASA's DC-8 Airborne Laboratory was deployed by the University of North Dakota/National Suborbital Education and Research Center, under contract with the NASA Wallops Flight Center.

References

[1] Jenniskens, P., et al., "Preparing for the Meteoritic Return of Stardust," *Workshop on Dust in Planetary Systems*, edited by H. Krueger and A. Graps, ESA SP 643, 2007, pp. 7–10.

[2] Harms, F., Waddell, P., Suess, M., and Roeser, H.-P., "On Sky Testing and Preliminary Sensor Alignment for the SOFIA Telescope," *Proceedings of SPIE: Ground-Based and Airborne Telescopes*, Vol. 6267, edited by L. M. Stepp, SPIE Publ., Bellingham, WA, 2006.

[3] "SBIG Operating Manual," Rev. 1.4, Santa Barbara Instrument Group, Santa Barbara, CA, 2004.

[4] Howell, S., *Handbook of CCD Astronomy*, Cambridge Univ. Press, Cambridge, England, U. K., 2000, p. 176.

[5] Jenniskens, P., "Observations of the Stardust Sample Return Capsule Entry with a Slit-Less Echelle Spectrograph," AIAA 46th Aerospace Science Meeting and Exhibit, AIAA Paper 2008-1210, 2008.

[6] Taylor, M. J., and Jenniskens, P., "Near-Infrared Spectroscopy of the Stardust Sample Return Capsule Entry: Detection of Carbon," *Journal of Spacecraft and Rockets*, Vol. 47, No. 6, 2010, pp. 878–883. doi:10.2514/1.38075

[7] Jacoby, G. H., Hunter, D. A., and Christian, C. A., "A Library of Stellar Spectra," *Astrophysical Journal, Supplement Series*, Vol. 56, 1984, pp. 257–281. doi:10.1086/190983

M. Wright
Guest Editor